# Additive Titanium Manufacturing to Repair Critically Sized Antebrachial Bone Defects in Two Dogs

S.D.S. Janssens[1] K. Willemsen[2,3] J. Magré[2,3] B.P. Meij[1]

[1] Department of Clinical Sciences, Faculty of Veterinary Medicine, Utrecht University, Utrecht, the Netherlands
[2] Department of Orthopaedics, University Medical Center Utrecht, Utrecht, the Netherlands
[3] 3D Lab, Division of Surgical Specialties, University Medical Center Utrecht,the Netherlands

**Address for correspondence** Sara Janssens, DVM, DECVS, Yalelaan 108, 3584 CM Utrecht, the Netherlands (e-mail: S.D.S.Janssens@uu.nl).

VCOT Open 2023;6:e75–e83.

## Abstract

Recent developments in the medical field of additive manufacturing (AM) have allowed the creation of patient-specific porous titanium implants for use in the medical field. With correct pore size such scaffolds are able to be integrated into surrounding bone. Two dogs were presented with atrophic non-union of the proximal ulna involving the elbow joint due to previous orthopaedic procedures with severe complications that led to segmental bone defects that were not expected to heal without a secondary intervention. Computed tomography (CT) was performed and porous scaffolds and saw guides were designed *in silico* and printed by AM. Osteotomies in adjacent healthy bone were guided by patient-specific three-dimensional (3D)-printed nylon saw guides allowing a perfect fit for the 3D-printed implant. In one case the scaffold was filled with bone morphogenic protein and held in place by two plates. In the other case the scaffold was filled with cancellous bone graft and held in place by a titanium plate that was part of the scaffold design. Both cases regained function and weight-bearing without lameness. Osseointegration of the implant was shown in both cases on follow-up CT and radiographs and macroscopically evident in the pores of the 3D implant after plate removal. One dog was euthanatized for unrelated disease and micro-CT revealed solid bone bridging through the inner scaffold tunnel.

This study showed the successful application of the design, fabrication and clinical use of a patient-specific 3D-printed titanium implant to repair segmental bone defects of the antebrachium in two dogs.

**Keywords**
- 3D printing
- patient-specific implants
- non-union
- dog

## Introduction

Failure of osteosynthesis can be caused by an inadequate mechanical or biological environment, or both. Biological inactivity at the fracture site, despite adequate fixation, may result in inadequate bone healing and is defined as a non-union.[1,2] A subclassification of non-union is atrophic non-union, which is characterized by complete absence of restorative processes.[2,3] Treatment of an atrophic non-union is often challenging and requires surgical debridement of all non-viable tissue. To stimulate bone regeneration and to bridge a segmental bone defect that is not expected to heal without a secondary (surgical) intervention, rigid fixation is of vital importance.[3] If the fracture non-union involves an articular surface, segmental bone bridging should preferably

**received**
September 29, 2022
**accepted after revision**
April 24, 2023

**DOI** https://doi.org/10.1055/s-0043-1769011.
**ISSN** 2625-2325.



Georg Thieme Verlag KG, Rüdigerstraße 14, 70469 Stuttgart, Germany

also restore anatomic alignment of the joint surface. To enhance biological activity, autogenous cortico-cancellous bone grafts together with recombinant human bone morphogenetic protein-2 (rhBMP-2) or rhBMP-7 can be used.[4,5] In addition, large segmental bone defects benefit from the use of free autogenous cortico-cancellous grafts (e.g. rib sections) or vascularised grafts from and adjacent paired bone, whenever possible.[6] In some cases of non-union, and due to a poor prognosis, high expenses and unsuccessful treatment attempts, a high degree of morbidity may prevail, with the end-point decision being amputation. However, recent innovations in additive manufacturing (AM) offer a surgical solution when off-the-shelf implants with fixed sizes fail to reach an acceptable solution to bridge a non-union with a segmental bone defect, especially in cases with involvement of a joint surface that requires accurate anatomic restoration.[7,8]

Additive manufacturing is used for rapid prototyping and small series manufacturing.[7] Digital three-dimensional (3D) models are *in silico* created by using medical imaging. Standard Digital Imaging and Communications in Medicine (DICOM) images are reconstructed to 3D models in readily available segmentation software. This AM technique enables the manufacturing of implants directly from a digital 3D stereolithography model by direct metal topographical printing using the technique of selective laser melting. The main advantages of this technique are the ability to manufacture complex 3D geometries, to develop scaffolds with well-controlled pore size, porosity and interconnecting pore size as well as an adequate resistance force, which is very difficult to accomplish through conventional manufacturing technologies.[9] This technique has a twofold effect on efficiency. It will reduce waiting time between diagnosis and surgery as well as a reduction in surgical time with improved gap bone healing.[7,8] The additional advantage of porous metals lies in their open space surface for the ingrowth of bone tissue, hence accelerating the osseointegration process.[9] Over the last decade, AM is increasingly used in both human and veterinary medicine and multiple case studies have been reported.[10–26] In veterinary surgery this technique has mainly been used for reconstruction of skull defects but recently, new applications for the treatment of hip dysplasia have been published.[27–30]

The aim of this study was to describe the implant design and the clinical use of patient-specific 3D-printed osteotomy guides, and patient-specific 3D-printed porous titanium implants to bridge segmental antebrachial non-unions in two dogs involving the elbow joint.

## Case Description

### Case 1

A 1-year-old, 40 kg, female, Bernese Mountain Dog was referred 11 weeks after bi-oblique dynamic proximal ulnar osteotomy (BOD-PUO) of the right antebrachium for elbow dysplasia with medial coronoid disease and incongruency. The osteotomy in the ulna was performed unusually close to the elbow joint. Three weeks after the BOD-PUO the dog developed a surgical site infection, which was treated with broad-spectrum antibiotic medications. Despite conservative management with antibiotic medications and non-steroidal anti-inflammatory drugs, the dog developed a persistent lameness of the right thoracic limb grade 4 out of 5, moderate-to-severe muscle atrophy of the antebrachial musculature and joint effusion of the elbow joint.[31] Concurrent orthopaedic abnormalities included bilateral subluxations of the hip joints due to hip dysplasia. Radiographic examination revealed an atrophic non-union of the right proximal ulna with malalignment and intra-articular extension (►**Fig. 1A**). There was severe osteoarthrosis with subchondral bone lesions, joint effusion and incongruency of the right elbow. Computed tomography (CT) of both forelimbs revealed a chronic osteolytic defect of 10 mm of the right proximal ulna and severe right elbow osteoarthritis with fragmentation of the medial coronoid process, incongruity and mineralization and erosion of cartilage and subchondral erosive lesions.

### Implant Design

A patient-specific 3D implant was designed to fill the segmental defect in the right ulna and restore the ulnar elbow joint alignment. To develop the patient-specific implant, first the DICOM files of the CT scan (250 mAs, 120 kV, 0.6 mm slice


**Fig. 1** (**A**) A 1-year-old Bernese Mountain dog (case 1) was presented with an atrophic non-union of the right proximal ulna, malalignment with intra-articular extension and severe elbow osteoarthrosis. (**B**) The left ulna (also showing elbow osteoarthrosis) was mirrored to obtain an approximation of the original anatomy of the right ulna for the design and additive manufacturing of a three-dimensional patient-specific implant (*blue*) for ulnar reconstruction. (**C**) Immediate postoperative radiograph showing the bridging titanium implant restoring elbow congruency and fixation with two plates. (**D**) Twenty months postoperative radiograph showing stable position of the implant.

thickness) were exported from the imaging archive system to Mimics (v21, Materialise NV., Leuven, Belgium) for anatomical segmentation. Standard bone threshold values (226 HU – upper threshold) were taken to segment the bone. The left ulna was mirrored to obtain an approximation of the original anatomy of the right ulna for the accomplishment of a 3D patient-specific implant for ulnar reconstruction (►**Fig. 1B**). Hereafter, the non-union was manually segmented together with a digitally grown resection margin that was used to simulate the minimal needed resection area to obtain straight osteotomies enhancing the press fit placement of the 3D patient-specific implant. Subsequently the anatomical models were transferred as stereolithography files to 3-matic software (v13, Materialise NV., Leuven, Belgium) in which the design took place. The proximal and distal resection guides were designed, to remove the irregular non-viable bony edges of the non-union. The resulting gap between the two osteotomies determined the size of the required implant (20 mm length × 18 mm in width). The ulnar reconstruction implant was designed as press fit porous titanium (70% porous, 500–600 µm pore size, Dodecahedron unit cell) to allow bony ingrowth at the implant bone interface. Additionally, the central region of the implant contained two holes for application of an autogenous cancellous bone graft together with demineralized bone matrix (►**Fig. 2A**).

## Production and Presurgical Planning

The osteotomy saw guides and the left and right ulna were 3D-printed in Nylon (PA12) on an EOS P110 printer (EOS, Krailling, Germany). The implant was 3D-printed in medical grade titanium alloy Ti-6Al-4V ELI grade 23 using direct

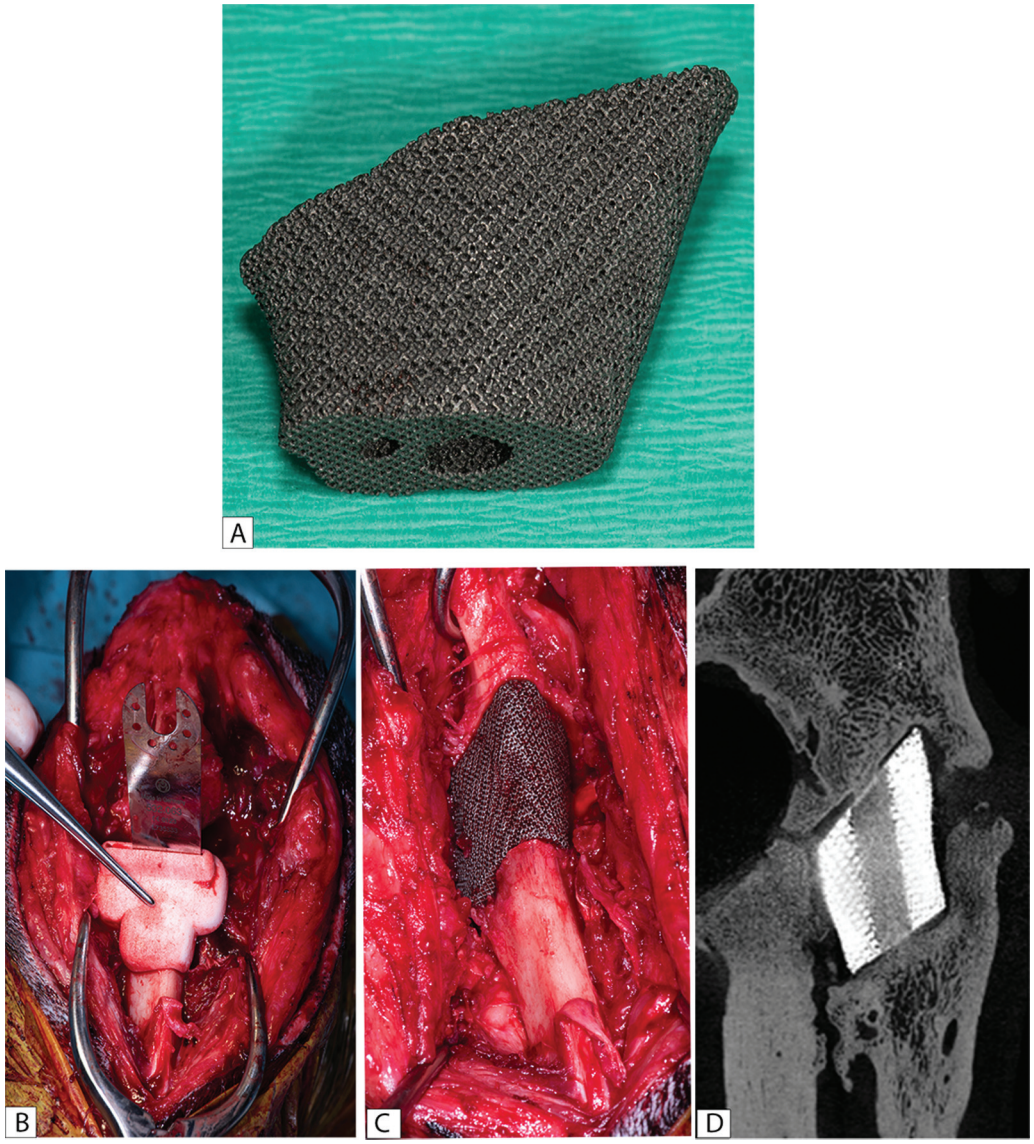


**Fig. 2** (**A**) Case 1: the ulna was reconstructed with a three-dimensional (3D)-printed porous titanium implant with central canals for the application of an autogenous cancellous bone graft with demineralized bone matrix. (**B**) Intraoperative view showing the 3D-printed surgical saw guide (*white*) that was applied on the caudal ulnar surface. (**C**) The implant was fitted in between both ulnar fragments and fixated with two plates (not shown). (**D**) Micro-computed tomography at 24 months postoperatively (after euthanasia). Bone ingrowth and bridging are evident on a sagittal median view through the central canal of the implant.

metal printing on a ProXDMP320 printer (3D Systems, Leuven, Belgium) by the process of selective laser melting of powders containing titanium using topographical printing. Post-processing included chronologically: hot-isostatic-pressing, screw wiretapping, polishing and manual cleaning. Rehearsal surgery was performed using the 3D-printed bone specimen together with the saw guides and titanium scaffold, allowing precise selection of the size and length of the plates and contouring to the bone and presurgical planning for the screw trajectories. Before surgery both the guides and the implant were manually cleaned, and standardized autoclave sterilized at the in-house sterilization facility.

### Surgery

The patient was placed in dorsal recumbency with the affected limb suspended and retracted caudally for draping. A caudal approach to the proximal shaft of the ulna was performed.[32] Subperiosteal elevation and medial retraction of the flexor carpi ulnaris muscle and lateral retraction of the extensor carpi ulnaris muscle exposed the ulnar shaft. After debridement of both fragments, the 3D-printed patient-specific surgical saw guides were applied to the caudal ulnar bone surface using manual press fit and with the help of a double pointed bone clamp. Perfect fit of the saw guide was confirmed before the distal and proximal osteotomies were performed with a 0.6 mm thick oscillating saw (DePuy Synthes, Johnson-Johnson, Oberdorf, Switzerland) (►**Fig. 2B**). Following removal of the ulnar non-union, the newly formed bone ends were inspected for viability and bleeding. The patient-specific 3D implant was embedded with the autogenous cancellous bone graft harvested from the ipsilateral tuberculum majus and mixed with artificially engineered demineralized bone matrix (Attrax Putty, Nuvasive, San Diego, California, United States). The titanium implant was fitted in between both ulnar fragments (►**Fig. 2C**) and after restoration of the ulnar alignment and elbow congruence a hybrid dynamic compression plate 3.5/2.7 mm (hybrid DCP [HDCP]) (DePuy Synthes, Johnson-Johnson, Oberdorf, Switzerland) was placed caudally on the tension side of the ulna under fluoroscopic guidance. An additional 2.7 mm DCP (DePuy Synthes, Johnson-Johnson, Oberdorf, Switzerland) was applied medially and fixed with two bicortical cortical screws to prevent medial displacement of the titanium implant. Before routine closure, $4 \times 32.5$ mg gentamycin sponges (Garacol, SERB SA, Brussels, Belgium) were applied locally around the implant.

### Follow-Up

Postoperative radiographs showed a stable construction (►**Fig. 1C**). At the 4 months postoperative check, there was clinical improvement in use of the right thoracic limb and CT revealed no changes with postoperative radiographs. At 5 months postoperatively, the dog developed a progressive worsening lameness at the right thoracic limb. Five out of seven cortical screws used with the caudal HDCP plate were broken. During surgical removal of the hybrid plate, inspection of the 3D implant showed a macroscopic stable embedding between the proximal and distal adjacent bone segments. Eleven months after surgery, the medial DCP plate was removed because of failure of the two screws and intra-operative inspection showed continued embedding of the 3D implant. At 20 months follow-up (after the initial surgery), the dog showed significant clinical improvement with minimal lameness compared to previous orthopaedic examinations. The 3D implant was radiologically stable in position with a radiolucent line around the entire implant (►**Fig. 1D**). Whether the radiolucent line was caused by failure of the implant to fully osseointegrate or by the Uberschwinger artefact (radiolucent halo around metal when there is a large density difference between adjacent objects) could not be determined.[33–35] There was a mild-to-moderate progression of the elbow joint osteoarthrosis. Two years postoperatively the dog developed right pelvic limb lameness. Radiographs of the stifle revealed an osteolytic process in the distal femur with aggressive characteristics. The owner elected euthanasia of the dog and consented to postmortem collection of the antebrachial segment. At the time of collection of the bone sample, it appeared that the implant was macroscopically completely integrated with the ulna segment. 3D micro-CT scan (VECTor6/CT system, MILabs B.V., Utrecht, the Netherlands) was obtained of the bone specimen with the following parameters: multi-circle 360 degrees acquisitions, tuber voltage of 55KV, tube current of 0.19 mA, exposure time of 75 ms per projection, angle increment of 0.5 degrees and 50 µm reconstructed isotropic voxel size using 3D Feldkamp filtered back-projection reconstruction. Micro-CT revealed bone in-growth in the medullar cavity of the porous segment (►**Fig. 2D**); however, ingrowth of bone in the smaller porous structure was too small for detection. Histopathology was performed on the collected antebrachial segment to study bone ingrowth. The formalin fixed samples were embedded in polymethylmethacrylate. The polymethylmethacrylate embedded plug was cut with a Leica 4 SP1600 Saw Microtome system (Leica) to yield 30 to 50 µm sections and these were stained with basic fuchsine-methylene blue. Overview pictures were made with a Thunder imaging system (Leica) and revealed that there was new bone formation present in the medullary cavity of the porous segment but absence of osseointegration in the smaller porous segment at the bone–implant interface (►**Fig. 3**).

### Case 2

A 4-year-old, 25 kg, male, Schapendoes, was presented with a history of a left-sided transverse olecranon fracture due to a traffic accident 3 years ago which was treated by open reduction and internal fixation and complicated by osteomyelitis. Implants were removed after 12 weeks and with physiotherapy the dog regained some weight-bearing function of the left thoracic limb with severe intermittent non-weight-bearing lameness. Two weeks before the presentation at the university, the dog suffered another road traffic accident and was therefore referred. Radiological examination revealed a chronic, complete, transverse, intra-articular non-union of the left olecranon and moderate osteoarthrosis of the elbow joint and subchondral sclerosis of the ulna (►**Fig. 4A**). A CT scan was performed as well as an arthrocentesis to assess whether there was an infectious arthritis. A chronic osteolytic defect of approximately 12 mm of the

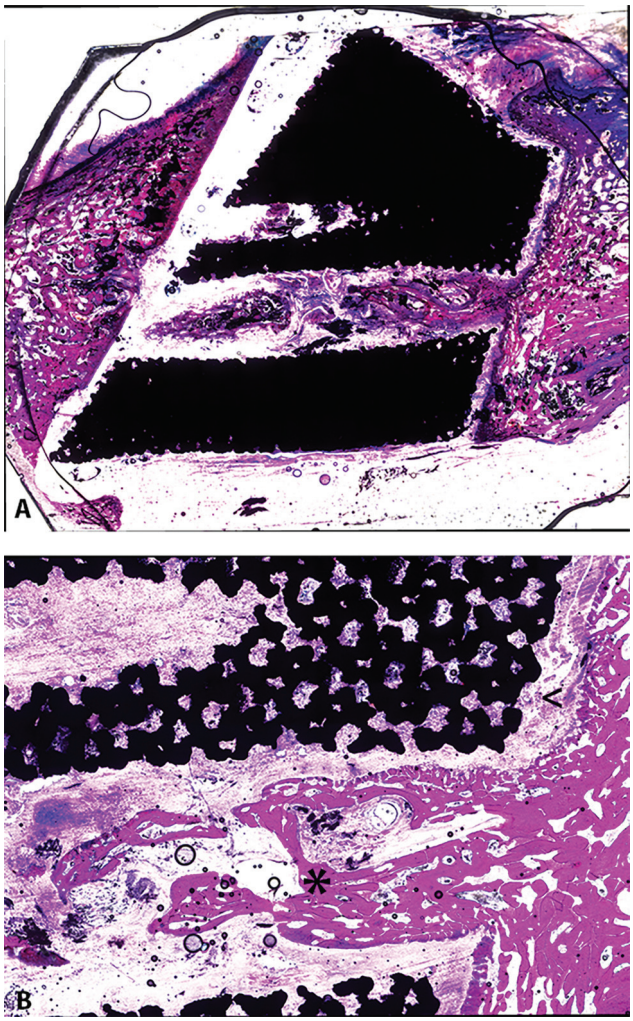


**Fig. 3** (**A**) Overview – New bone formation present in the medullary cavity of the porous segment (*). (**B**) Absence of osseointegration in the smaller porous segment at the bone–implant interface (<).

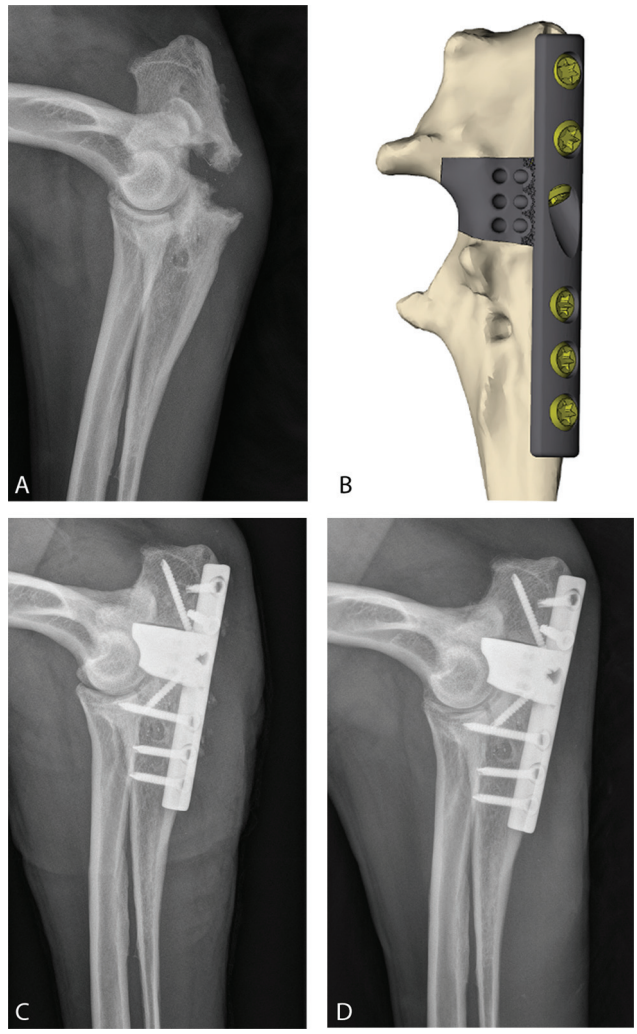


**Fig. 4** (**A**) A 4-year-old Schapendoes (case 2) was presented with a chronic, complete, transverse, intra-articular non-union of the left olecranon and a moderate amount of osteoarthrosis of the elbow joint. (**B**) Design of the three-dimensional (3D) patient-specific implant with incorporation of a 3D-printed titanium plate with seven holes. Immediate (**C**) and 6 weeks (**D**) postoperative radiographs showing stable presentation of the bridging porous implant and plate that was fixed with five 2.7 mm and two 2.4 mm titanium screws. The semilunar ulnar trochlea has been restored resulting in elbow congruency.

proximal left ulna was present with concurrent bilateral signs of medial coronoid disease. Prior to surgery, and at 6 weeks and 10 weeks after surgery, ground reaction forces were measured with a quartz crystal piezoelectric force plate (Kistler type 9261, Charnwood Dynamics Limited, Rothley, UK) together with the Kistler 9865E charge amplifiers, as described previously.[36,37] Measurements were obtained with a frequency of 100 Hz. Ground reaction forces were measured in the mediolateral (Fx), craniocaudal (Fy), and vertical (Fz) direction. The presurgical measurement revealed a $Fz_{max}$ of 12 N/kg bodyweight of the right thoracic limb and $Fz_{max}$ of 0 N/kg bodyweight of the left thoracic limb (i.e. no weight bearing).

### Implant Design

Saw guides and a patient-specific 3D implant were designed from the CT images in a similar manner as in case 1. The ulnar reconstruction implant was manufactured as press fit porous titanium (70% porous, 500–600 µm pore size, Dodecahedron unit cell) to allow bony ingrowth at the implant bone interface (►**Fig. 5A**). The porous titanium implant was modified in comparison to case 1 by incorporating a 3D-printed titanium 6-hole 2.7 mm plate on the caudal side and designing two drill guides for the screws to capture the screw direction and screw length for optimal bone stock in the proximal and distal fragment (►**Fig. 4B**). Additionally, the central region of the bone-bridging-implant contained 1 hole for application of an autogenous cancellous bone graft. The surgical saw guides and drill guides were 3D-printed in Nylon (PA12) on an EOS P110 printer (EOS, Krailling, Germany) and the implant was 3D-printed in medical grade titanium alloy Ti-6Al-4V ELI grade 23 using direct metal printing on a ProXDMP320 printer (3D Systems, Leuven, Belgium). Post-processing of the implant included polishing and HIP treatment. Before surgery, both, the guides and the implant were manually cleaned and sterilized.

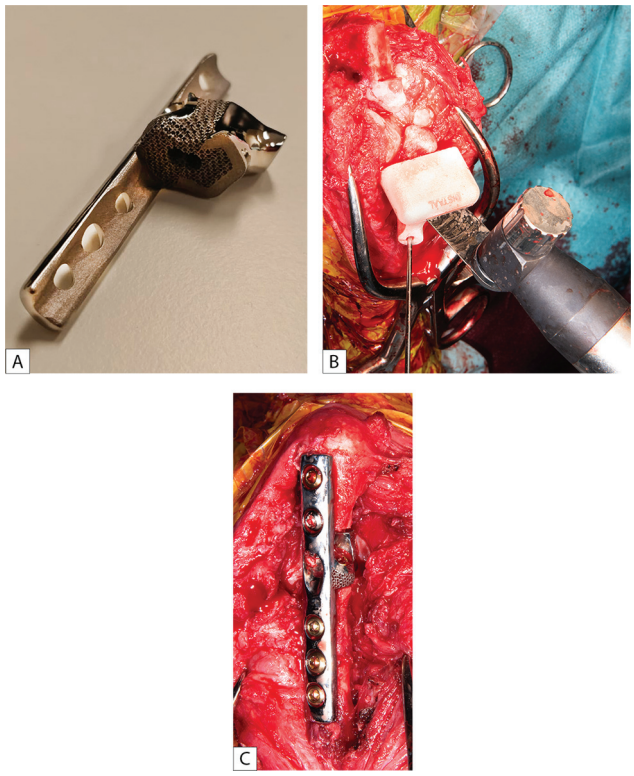

**Fig. 5** (**A**) Case 2: the ulna was reconstructed with a three-dimensional (3D)-printed titanium implant consisting of an ulnar bridging porous part and a caudal 2.7 mm plate. The porous part contained 1 hole for application of an autogenous cancellous bone graft and two screw holes for 2.4 mm titanium screws. (**B**) Intraoperative view showing the 3D-printed surgical saw guide (*white*) that was held in place with a Kirschner wire at the time of the osteotomy. (**C**) The patient-specific 3D implant was fitted in between both ulnar fragments and fixed with the plate and seven screws.

### Surgery

Surgical approach to the caudal side of the ulna was performed in a similar fashion as in case 1. The anconeal process was used as lever to dislocate the articulating surfaces to gain better visualization of the proximal fragment and to better assess the intra-articular ulnar defect. After debridement of both fragments, the 3D-printed patient-specific osteotomy saw guides were applied to the caudal ulnar bone surface and when perfect fit was confirmed, the saw guides were temporarily fixed with 1.6 mm Kirschner wires (►**Fig. 5B**). Distal and proximal osteotomies were performed with a 0.6 mm thick oscillating saw and new bone formations on the caudal and medial part of the ulna were removed. The implant was filled through the central hole with an autogenous cancellous bone graft harvested from the ipsilateral tuberculum majus and was then fitted in between both ulnar fragments. First the implant was fixated to the proximal fracture fragment using the proximal drill guide by placing a central 2.4 mm titanium cortex screw (Unilock, DePuy Synthes, Johnson-Johnson, Oberdorf, Switzerland). After reduction in the anconeal process and alignment of the proximal and distal ulnar fragments, fixation of the most distal part of the plate occurred using the distal drill guide and placing three 2.7 mm titanium screws (Kyon, Zürich, Switzerland) under fluoroscopic guidance of elbow congruency. Fixation of the plate was completed by applying one 2.7 mm titanium screw (Kyon, Zürich, Switzerland) and one 2.7 mm 316 L stainless steel cortical screw using the proximal drill guide (►**Fig. 5C**). Before closure an autologous bone graft was applied around the implant.

### Follow-Up

Postoperative radiographs showed a stable construction (►**Fig. 4C**). The patient was discharged with a Modified Robert Jones bandage containing a splint. Bandage changes were performed on a weekly base for 6 weeks. The dog started to use the thoracic limb during the ensuing 6-week period of bandage changes and after removal a gradual return to full weight bearing without lameness occurred and was confirmed at 15-month follow-up. Radiographs at 6 and 10 weeks after surgery showed a stable presentation of the metallic implants and congruent elbow with osteoarthrotic changes similar to previous studies (►**Fig. 4D**). Six- and ten-weeks postoperative force plate analysis was rechecked. At 6 weeks $Fz_{max}$ of the left thoracic limb was 3.5 N/kg and $Fz_{max}$ of the right thoracic limb was 9 N/kg. Measurements were repeated at 10 weeks postoperatively and showed an increase in $Fz_{max}$ of the left thoracic limb of 5.5 N/kg and a $Fz_{max}$ of the right thoracic limb of 8 N/kg.

## Discussion

This report described the use and feasibility of additive titanium manufacturing to create a 3D patient-specific implant for repair of atrophic non-unions with segmental antebrachial bone defects in dogs with incorporating a polished joint segment in one case. Both patients were presented with atrophic non-unions in close vicinity of the elbow joint as a result of prior unsuccessful osteosyntheses. The alternative surgical options for these cases were either limb amputation or the use of fixed size off-the-shelf implants. The latter were not considered optimal due to the absence of a complete articular surface or accurate anatomical reconstruction which would result in severe morbidity.[38] Reconstruction of the ulna, and in one case the joint surface of the elbow, with the 3D patient-specific implants, led to functional limb use and excellent clinical outcome in both cases.

Both implants were made of porous titanium scaffold with a hollow centre intended to allow bone ingrowth and therefore permanent osseointegration of the implant in the ulna. However, in case 1 bone ingrowth was seen macroscopically around the 3D-printed scaffold but on radiographs a radiolucent line remained around the entire implant. Whether the radiolucent line was caused by failure of the implant to fully osseointegrate or by the Uberschwinger artefact (radiolucent halo around metal when there is a large density difference between adjacent objects) could not be determined on the radiographs. Uberschwinger artefact may simulate loosening of orthopaedic devices.[33–35]

Postmortem histology of the bone specimen revealed new bone formation in the medullary cavity of the porous

segment, but absence of osseointegration in the smaller porous segment at the bone–implant interface of the scaffold in the ulnar bone. In previous experimental studies micromovements between bone and implant inhibited bony ingrowth and led to the development of a fibrous membrane.[39] The strength in implant embedding is increased by bone ingrowth.[40–43] Li and colleagues concluded that increase in porosity and pore size of titanium alloy implants have a positive influence on osteoconductive properties.[43] Biofunctionalizing surface treatments like alkali-acid-heat treatment (AlAcH) can improve the apatite forming ability of AM scaffolds, and have a positive effect on cell attachment, cell proliferation and osteogenic gene expression. The relationship between these properties and the bone–implant biomechanics is, however, not trivial.[44–47]

In the second case with a chronic non-union and a segmental bone defect extending into the elbow joint, the use of an interlocking nail, hybrid external fixator or a trans articular external fixator, plate fixation or a combination of these techniques would not have resulted in a clinical anatomic union. The use of a porous 3D patient-specific implant combined with a polished joint segment and a plate on the tension side of the ulna resulted in a stable construction.

In both cases, the dogs started to use the limb again and full weight bearing was achieved with good clinical function. However, in case 1 the bone bridging implant was not connected to the plates that acted as buttress plates, making them probably more susceptible to mechanical failure. This resulted in multiple failures of plate screws which necessitated plate and screw removal at 5 and 11 months after surgery. At the time of plate removal, it was possible to macroscopically assess osseointegration of the porous implant and this was found to be a solid component of the ulna and micro-CT at 24 months confirmed bone bridging through the central hole in the titanium scaffold. At that time bone bridging was not complete caudal to the implant which may be due to remaining micromotion on the tension site of the ulna or simply because the dog did not survive long enough because of euthanasia for multiple concurrent orthopaedic abnormalities.

Ongoing insight in patient-specific implants and their application together with experience of the implant failures in case 1 resulted in adaptations of the design of the implant in case 2. The modification existed of incorporating a 3D-printed 2.7 mm titanium plate on the caudal site of the porous titanium implant as well as the design of two screw holes through the porous implant itself. The porous scaffold between the bone parts contained one central hole for application of a cancellous bone graft and two screw holes so the implant itself was also fixated to the bone but was also an integral part with the caudal plate that was additionally fixated with screws to the ulna. The incorporation of a plate on the caudal side of the scaffold has added stability to the construct and the design likely reduced stress. In addition, in case 2 drill guides were designed presurgically for screw placement which allowed precise selection of screw direction and screw length in relation to the bone stock avoiding the joint surface of the elbow. This may have led to distribution of scaffold and plate fixation forces, again reducing stress shielding, and therefore help bone and implant survival.

Force plate analysis was performed in case 2 and showed preoperatively overcompensation of the right thoracic limb. Postoperatively at 6 weeks there was a noticeable difference in $Fz_{max}$ between both the left and the right thoracic limbs, whereas at 10 weeks the absolute difference in $Fz_{max}$ between both thoracic limbs decreased. One can conclude that these results indicate a clinical improvement of the left thoracic limb lameness. However, a force plate analysis is a snapshot of a particular moment in time and provides little information about the use of the limb during the entire day, e.g., while playing, lying down and standing. Because the limited value of force plate gait analysis to evaluate the complete function of the dog it is not routinely used in clinical practice; however, in this case the gait analysis objectively confirmed improvement in the functional use of the limb from preoperative to postoperative.[48]

The patient-specific nature of the implants may cause an inherent delay in the availability of implants, and this should be considered in the surgical planning and when addressing the owner's expectations. In these two cases, the lead time for the implants between imaging and surgery was approximately 3 months and is due to time needed for design, feedback to the surgeon and adapting the design, manufacturing of the implant, post-processing and quality control, transportation and sterilization procedures. Protocols and algorithms can be written to have a faster design process.[49]

This report has several limitations. This is a description of two cases with similar lesions in nature and ongoing insight and experiences with case 1 have changed the design for case 2. Imaging at follow-up is not uniform. Minimal requirements for follow-up are radiography to monitor implant position and implant failure; however, CT is considered of added benefit to assess bone in-growth in the titanium scaffold. For more detail on bone ingrowth, micro-CT and histology are recommended when bone specimens become available. It is concluded that the use of additive titanium manufacturing to create an implant with a polished joint surface to restore the elbow joint, to fill the segmental defect to stabilize the non-union and to promote osseointegration through the hollow centre is a novel technique and may be used to treat segmental bone defects in dogs.

## Conclusion

Atrophic non-unions with a segmental ulnar bone defect in close vicinity of the elbow joint in dogs are difficult to treat. The use of additive titanium manufacturing can help to create an implant with a polished joint surface to restore the elbow joint.

**Conflict of Interest**
None declared.

## References

1 Schmal H, Brix M, Bue M, et al; Danish Orthopaedic Trauma Society. Nonunion - consensus from the 4th annual meeting of the Danish Orthopaedic Trauma Society. EFORT Open Rev 2020;5 (Suppl 1):46–57

2 Frölke JPM, Patka P. Definition and classification of fracture nonunions. Injury 2007;38(Suppl 2):S19–S22
3 Delayed unions, nonunions, and malunions. In: Tobias KM, Johnston SA, eds. Veterinary Surgery Small Animal. St. Louis: WB Saunders; 2012:647–656
4 Faria ML, Lu Y, Heaney K, Uthamanthil RK, Muir P, Markel MD. Recombinant human bone morphogenetic protein-2 in absorbable collagen sponge enhances bone healing of tibial osteotomies in dogs. Vet Surg 2007;36(02):122–131
5 Kirker-Head CA, Boudrieau RJ, Kraus KH. Use of bone morphogenetic proteins for augmentation of bone regeneration. J Am Vet Med Assoc 2007;231(07):1039–1055
6 Calori GM, Mazza E, Colombo M, Ripamonti C. The use of bone-graft substitutes in large bone defects: any specific needs? Injury 2011;42(2, Suppl 2):S56–S63
7 Koptyug A, Rännar L, Bäckström M, Fager Franzén S, Dérand P. Additive manufacturing technology applications targeting practical surgery. Int J Life Sci Med Res 2013;3(01):15–24
8 Salmi M. Medical applications of additive manufacturing in surgery and dental care [Ph.D. dissertation]. Helsinki; Aalto University; 2013
9 Wang X, Xu S, Zhou S, et al. Topological design and additive manufacturing of porous metals for bone scaffolds and orthopaedic implants: a review. Biomaterials 2016;83:127–141
10 Farré-Guasch E, Wolff J, Helder MN, Schulten EA, Forouzanfar T, Klein-Nulend J. Application of additive manufacturing in oral and maxillofacial surgery. J Oral Maxillofac Surg 2015;73(12):2408–2418
11 Ciocca L, Fantini M, De Crescenzio F, Corinaldesi G, Scotti R. Direct metal laser sintering (DMLS) of a customized titanium mesh for prosthetically guided bone regeneration of atrophic maxillary arches. Med Biol Eng Comput 2011;49(11):1347–1352
12 Ciocca L, Donati D, Ragazzini S, et al. Mesenchymal stem cells and platelet gel improve bone deposition within CAD-CAM custom-made ceramic HA scaffolds for condyle substitution. BioMed Res Int 2013;2013:549762. https://www.hindawi.com/journals/bmri/2013/549762
13 Li J, Hsu Y, Luo E, Khadka A, Hu J. Computer-aided design and manufacturing and rapid prototyped nanoscale hydroxyapatite/polyamide (n-HA/PA) construction for condylar defect caused by mandibular angle ostectomy. Aesthetic Plast Surg 2011;35(04):636–640
14 Mangano C, Piattelli A, d'Avila S, et al. Early human bone response to laser metal sintering surface topography: a histologic report. J Oral Implantol 2010;36(02):91–96
15 Mangano FG, De Franco M, Caprioglio A, Macchi A, Piattelli A, Mangano C. Immediate, non-submerged, root-analogue direct laser metal sintering (DLMS) implants: a 1-year prospective study on 15 patients. Lasers Med Sci 2014;29(04):1321–1328
16 Mueller AA, Paysan P, Schumacher R, et al. Missing facial parts computed by a morphable model and transferred directly to a polyamide laser-sintered prosthesis: an innovation study. Br J Oral Maxillofac Surg 2011;49(08):e67–e71
17 Rohner D, Hutmacher DW, Cheng TK, Oberholzer M, Hammer B. In vivo efficacy of bone-marrow-coated polycaprolactone scaffolds for the reconstruction of orbital defects in the pig. J Biomed Mater Res B Appl Biomater 2003;66(02):574–580
18 Saijo H, Igawa K, Kanno Y, et al. Maxillofacial reconstruction using custom-made artificial bones fabricated by inkjet printing technology. J Artif Organs 2009;12(03):200–205
19 Sándor GK, Tuovinen VJ, Wolff J, et al. Adipose stem cell tissue-engineered construct used to treat large anterior mandibular defect: a case report and review of the clinical application of good manufacturing practice-level adipose stem cells for bone regeneration. J Oral Maxillofac Surg 2013;71(05):938–950
20 Sándor GK, Numminen J, Wolff J, et al. Adipose stem cells used to reconstruct 13 cases with cranio-maxillofacial hard-tissue defects. Stem Cells Transl Med 2014;3(04):530–540
21 Sun Y, Luebbers HT, Agbaje JO, et al. Accuracy of upper jaw positioning with intermediate splint fabrication after virtual planning in bimaxillary orthognathic surgery. J Craniofac Surg 2013;24(06):1871–1876
22 Xu H, Han D, Dong JS, et al. Rapid prototyped PGA/PLA scaffolds in the reconstruction of mandibular condyle bone defects. Int J Med Robot 2010;6(01):66–72
23 Wang G, Li J, Khadka A, Hsu Y, Li W, Hu J. CAD/CAM and rapid prototyped titanium for reconstruction of ramus defect and condylar fracture caused by mandibular reduction. Oral Surg Oral Med Oral Pathol Oral Radiol 2012;113(03):356–361
24 Wolff J, Sándor GK, Miettinen A, et al. GMP-level adipose stem cells combined with computer-aided manufacturing to reconstruct mandibular ameloblastoma resection defects: experience with three cases. Ann Maxillofac Surg 2013;3(02):114–125
25 Jardini AL, Larosa MA, de Carvalho Zavaglia CA, et al. Customised titanium implant fabricated in additive manufacturing for craniomaxillofacial surgery: this paper discusses the design and fabrication of a metallic implant for the reconstruction of a large cranial defect. Virtual Phys Prototyp 2014;9(02):115–125
26 Willemsen K, Nizak R, Noordmans HJ, Castelein RM, Weinans H, Kruyt MC. Challenges in the design and regulatory approval of 3D-printed surgical implants: a two-case series. Lancet Digit Health 2019;1(04):e163–e171
27 James J, Oblak ML, Zur Linden AR, James FMK, Phillips J, Parkes M. Schedule feasibility and workflow for additive manufacturing of titanium plates for ranioplasty in canine skull tumors. BMC Vet Res 2020;16(01):180
28 Harrysson OL, Marcellin-Little DJ, Horn TJ. Applications of metal additive manufacturing in veterinary orthopedic surgery. JOM 2015;67(03):647–654
29 Golafshan N, Willemsen K, Kadumudi FB, et al. 3D-printed regenerative magnesium phosphate implant ensures stability and restoration of hip dysplasia. Adv Healthc Mater 2021;10 (21):e2101051
30 Willemsen K, Tryfonidou M, Sakkers R, et al. Patient-specific 3D-printed shelf implant for the treatment of hip dysplasia: anatomical and biomechanical outcomes in a canine model. J Orthop Res 2022;40(05):1154–1162
31 Vasseur PB, Johnson AL, Budsberg SC, et al. Randomized, controlled trial of the efficacy of carprofen, a nonsteroidal anti-inflammatory drug, in the treatment of osteoarthritis in dogs. J Am Vet Med Assoc 1995;206(06):807–811
32 Johnson KA. Piermattei's Atlas of Surgical Approaches to the Bones and Joints of the Dog and Cat. 5th ed. Philadelphia: PA Saunders; 2004:338–341
33 Mattoon JS. Digital radiography. Vet Comp Orthop Traumatol 2006;19(03):123–132
34 McLear RC, Handmaker H, Schmidt W, Walls C, Gottfried S, Siegel E. "Uberschwinger" or "Rebound effect" artifact in computed radiographic imaging of metallic implants in veterinary medicine. Vet Radiol Ultrasound 2004;45:266
35 Tan TH, Boothroyd AE. Uberschwinger artefact in computed radiographs. Br J Radiol 1997;70(832):431
36 Suwankong N, Meij BP, Van Klaveren NJ, et al. Assessment of decompressive surgery in dogs with degenerative lumbosacral stenosis using force plate analysis and questionnaires. Vet Surg 2007;36(05):423–431
37 Tellegen AR, Willems N, Tryfonidou MA, Meij BP. Pedicle screw-rod fixation: a feasible treatment for dogs with severe degenerative lumbosacral stenosis. BMC Vet Res 2015;11:299
38 Long M, Rack HJ. Titanium alloys in total joint replacement—a materials science perspective. Biomaterials 1998;19(18): 1621–1639
39 Goodman S, Aspenberg P. Effect of amplitude of micromotion on bone ingrowth into titanium chambers implanted in the rabbit tibia. Biomaterials 1992;13(13):944–948


 

40 Wang H, Su K, Su L, Liang P, Ji P, Wang C. Comparison of 3D-printed porous tantalum and titanium scaffolds on osteointegration and osteogenesis. Mater Sci Eng C 2019;104:109908
41 Tanzer M, Chuang PJ, Ngo CG, Song L, TenHuisen KS. Characterization of bone ingrowth and interface mechanics of a new porous 3D printed biomaterial: an animal study. Bone Joint J 2019;101-B (6_Supple_B):62–67
42 Reints Bok TE, Willemsen K, van Rijen MHP, Grinwis GCM, Tryfonidou MA, Meij BP. Instrumented cervical fusion in nine dogs with caudal cervical spondylomyelopathy. Vet Surg 2019;48 (07):1287–1298
43 Li JP, Habibovic P, van den Doel M, et al. Bone ingrowth in porous titanium implants produced by 3D fiber deposition. Biomaterials 2007;28(18):2810–2820
44 Amin Yavari S, van der Stok J, Chai YC, et al. Bone regeneration performance of surface-treated porous titanium. Biomaterials 2014;35(24):6172–6181
45 Wauthle R, van der Stok J, Amin Yavari S, et al. Additively manufactured porous tantalum implants. Acta Biomater 2015;14:217–225
46 Wang H, Su K, Su L, Liang P, Ji P, Wang C. The effect of 3D-printed $Ti_6Al_4V$ scaffolds with various macropore structures on osteointegration and osteogenesis: A biomechanical evaluation. J Mech Behav Biomed Mater 2018;88:488–496
47 Søballe K, Hansen ES, B-Rasmussen H, Jørgensen PH, Bünger C. Tissue ingrowth into titanium and hydroxyapatite-coated implants during stable and unstable mechanical conditions. J Orthop Res 1992;10(02):285–299
48 Hielm-Björkman AK, Rita H, Tulamo RM. Psychometric testing of the Helsinki chronic pain index by completion of a questionnaire in Finnish by owners of dogs with chronic signs of pain caused by osteoarthritis. Am J Vet Res 2009;70(06):727–734
49 Popescu D, Lăptoiu D, Hadăr A, Ilie C, Pârvu C. Workflow for additive manufacturing of an individualized surgical template. Proceedings in Manufacturing Systems 2015;10(03):131–140

 